Regular Article

Inelastic processes in collisions of lithium positive ions with hydrogen anions and atoms[⋆]

Andrey K. Belyaev[1,2,a], Svetlana A. Yakovleva[1,2], and Wolfgang P. Kraemer[2]

[1] Department of Theoretical Physics and Astronomy, Herzen University, St. Petersburg 191186, Russia
[2] Max-Planck Institute for Astrophysics, Postfach 1371, 85741 Garching, Germany

ⓒ The Author(s) 2017. This article is published with open access at Springerlink.com

Abstract. Inelastic processes in the low-energy collisions $Li^{3+} + H^-$, $Li^{2+} + H$, $Li^{2+} + H^-$ and $Li^+ + H$ are investigated for all collisional channels with the excited ionic lithium states $Li^{2+}(nl)$ and $Li^+(1s\,nl)$ up to and including the corresponding ion-pair states for the temperature range 1000–20 000 K. For all possible processes in the $Li^{3+} + H^-$ and $Li^{2+} + H$ collisions inelastic cross sections and rate coefficients are calculated for the transitions between the ion-pair channel $Li^{3+} + H^-$ and the 35 below lying contributing $Li^{2+}(nl) + H$ channels. It is found that the highest values of cross sections and rate coefficients are obtained for the recombination processes and their inverse, the ion-pair formation processes, involving the $Li^{2+}(3l)$, $Li^{2+}(4l)$, and $Li^{2+}(5l)$ states. For the processes in the $Li^{2+} + H^-$ and $Li^+ + H$ collisions, cross sections and rate coefficients are calculated for all transitions between 34 $Li^+(1s\,nl) + H$ channels lying below $Li^{2+} + H^-$ plus this ion-pair channel. In this case the highest rate coefficients correspond to the recombination processes with the $Li^+(1s3l\ ^{1,3}L)$ and $Li^+(1s4l\ ^{1,3}L)$ final states, as well as their inverse processes of ion-pair production. Rate coefficient values for these most efficient processes are rather high, of the order of $10^{-8}\,cm^3/s$. This leads to total recombination rate coefficients in $Li^{3+} + H^-$ and $Li^{2+} + H^-$ collisions with values larger than $10^{-7}\,cm^3/s$.

1 Introduction

Collisions of multiply charged ions with atoms, ions, molecules, clusters, fullerenes, and surfaces have attracted a great deal of attention for decades, see, e.g., [1–3]. This is motivated by the necessity of an understanding of fundamental inelastic collision dynamics, as well as the needs of detailed cross sections and rate coefficients in some other research fields. The latter include inelastic collision processes in interactions of charged ion beams with plasma in fusion experiments, as well as with a residual gas in an accelerator storage ring. Collisions with multiply charged ions are also important in astrophysics, for example, collisions of solar-wind ions with atomic systems from the interstellar media which lead to charge exchange, excitation and de-excitation processes. A special interest exists in collisions between positive and negative ions, in particular, with hydrogen anions, collisions leading to neutralization processes. Recently, this kind of interest has been growing up due to the experiments carrying out within the Double ElectroStatic Ion Ring ExpEriment (DESIREE) project [4,5], see also [6] for the CSR

project and [7] for the RICE project. Among other processes, the experiments treat neutralization processes in collisions between cations and anions.

Lithium–hydrogen collisions are of interest, in particular, due to their importance for non-local thermodynamic equilibrium (non-LTE) modelings of cool stellar atmospheres (see, e.g., reviews [8–10], and references therein). It has been shown theoretically in reference [11] that the mutual neutralization processes $Li^+ + H^- \rightarrow Li(nl) + H(1s)$, as well as their inverse processes, the ion-pair production, are important for non-LTE modelings of lithium spectra in cool stellar atmospheres, which are in turn important for determining absolute and relative abundances of lithium. The mutual neutralization processes in $Li^+ + H^-$ collisions have been studied theoretically in references [12,13]; a maximum rate coefficient of the order of $10^{-7}\,cm^3/s$ was obtained. The excitation and de-excitation processes in $Li + H$ collisions have been treated theoretically in reference [14]. Inelastic processes in collisions of multiply charged lithium ions with hydrogen atoms and anions are much less studied. Inelastic processes involving the ground and the low-lying molecular states of the LiH^+ quasi-molecule, that is, the states asymptotically correlated to the interactions $Li^+ + H$, $Li(2s) + H^+$, $Li^*(nl = 2s, 2p, 3s, 3p) + H^+$, $Li^+ + H^*(n = 2, 3)$ have been recently studied in theoretical papers [15,16] (see also references therein). To the

Table 1. LiH^{2+}($^1\Sigma^+$) scattering channels and asymptotic energies (J-average experimental values taken from NIST [29]) with respect to the asymptote of the ground-state Li^{2+} ion interacting with an H atom.

j	Scattering (atomic) channels	Asymptotic energies (eV)
1	Li^{2+} $(1s\ ^2S)$ + H $(1s\ ^2S)$	0.0000000
2	Li^{2+} $(2s\ ^2S)$ + H $(1s\ ^2S)$	91.839612
3	Li^{2+} $(2p\ ^2P)$ + H $(1s\ ^2S)$	91.841804
4	Li^{2+} $(3s\ ^2S)$ + H $(1s\ ^2S)$	108.848175
5	Li^{2+} $(3p\ ^2P)$ + H $(1s\ ^2S)$	108.848824
6	Li^{2+} $(3d\ ^2D)$ + H $(1s\ ^2S)$	108.849403
7	Li^{2+} $(4s\ ^2S)$ + H $(1s\ ^2S)$	114.801041
8	Li^{2+} $(4p\ ^2P)$ + H $(1s\ ^2S)$	114.801315
9	Li^{2+} $(4d\ ^2D)$ + H $(1s\ ^2S)$	114.801560
10	Li^{2+} $(4f\ ^2F)$ + H $(1s\ ^2S)$	114.801664
11	Li^{2+} $(5s\ ^2S)$ + H $(1s\ ^2S)$	117.556309
12	Li^{2+} $(5p\ ^2P)$ + H $(1s\ ^2S)$	117.556449
13	Li^{2+} $(5d\ ^2D)$ + H $(1s\ ^2S)$	117.556574
14	Li^{2+} $(5f\ ^2F)$ + H $(1s\ ^2S)$	117.556628
15	Li^{2+} $(5g\ ^2G)$ + H $(1s\ ^2S)$	117.556658
16	Li^{2+} $(6s\ ^2S)$ + H $(1s\ ^2S)$	119.052973
17	Li^{2+} $(6p\ ^2P)$ + H $(1s\ ^2S)$	119.053054
18	Li^{2+} $(6d\ ^2D)$ + H $(1s\ ^2S)$	119.053126
19	Li^{2+} $(6f\ ^2F)$ + H $(1s\ ^2S)$	119.053157
20	Li^{2+} $(6g\ ^2G)$ + H $(1s\ ^2S)$	119.053174
21	Li^{2+} $(6h\ ^2H)$ + H $(1s\ ^2S)$	119.053185
22	Li^{2+} $(7s\ ^2S)$ + H $(1s\ ^2S)$	119.955402
23	Li^{2+} $(7p\ ^2P)$ + H $(1s\ ^2S)$	119.955453
24	Li^{2+} $(7d\ ^2D)$ + H $(1s\ ^2S)$	119.955499
25	Li^{2+} $(7f\ ^2F)$ + H $(1s\ ^2S)$	119.955518
26	Li^{2+} $(7g\ ^2G)$ + H $(1s\ ^2S)$	119.955529
27	Li^{2+} $(7h\ ^2H)$ + H $(1s\ ^2S)$	119.955536
28	Li^{2+} $(7i\ ^2I)$ + H $(1s\ ^2S)$	119.955541
29	Li^{2+} $(8s\ ^2S)$ + H $(1s\ ^2S)$	120.541107
30	Li^{2+} $(8p\ ^2P)$ + H $(1s\ ^2S)$	120.541142
31	Li^{2+} $(8d\ ^2D)$ + H $(1s\ ^2S)$	120.541172
32	Li^{2+} $(8f\ ^2F)$ + H $(1s\ ^2S)$	120.541185
33	Li^{2+} $(8g\ ^2G)$ + H $(1s\ ^2S)$	120.541192
34	Li^{2+} $(8h\ ^2H)$ + H $(1s\ ^2S)$	120.541197
35	Li^{2+} $(8i\ ^2I)$ + H $(1s\ ^2S)$	120.541200
36	Li^{2+} $(8k\ ^2K)$ + H $(1s\ ^2S)$	120.541203
i	Li^{3+} + H$^-$ $(1s^2\ ^1S)$	121.700155

best of our knowledge, the processes involving higher-lying states, that is, the states correlated to the Li^{+*} + H and Li^{2+} + H$^-$ channels, as well as the states correlated to the Li^{2+*} + H and Li^{3+} + H$^-$ channels, have not been treated so far. Since nowadays it is generally accepted that inelastic processes in heavy-particle collisions with hydrogen atoms and negative ions deserve more detailed consideration, especially, inelastic processes with high rate coefficients, this motivated us to study inelastic processes in collisions of lithium positive ions with hydrogen negative ions and neutral atoms. The interactions between multiply charged lithium ions and H$^-$ are obviously stronger compared to singly charged Li$^+$ and the corresponding collision processes are therefore expected to have higher rate coefficients.

Thus, in the present study, the role of the H$^-$ ion in collisions with the multiply charged lithium ions Li^{3+}

and Li^{2+} is studied. For this purpose inelastic cross sections and rate coefficients for the charge-recombination (electron-transfer) processes as well as their inverse reactions, the ion-pair formation processes, according to Li^{Z+} + H$^-$ $\rightleftharpoons$ Li$^{(Z-1)+}$ + H (with $Z = 3, 2$) are investigated. In particular, for the recombination process in Li^{3+} + H$^-$ collisions and its inverse the cross sections and rate coefficients for all transitions between the ion-pair channel Li^{3+} + H$^-$ and the below lying contributing Li^{2+}($nl\ ^2L$) + H channels are determined (see Tab. 1). And similarly for Li^{2+} + H$^-$ and Li$^+$ + H cross sections and rate coefficients are calculated for the transitions between the corresponding ion-pair channel and all the relevant below lying Li$^+$($1snl\ ^{1,3}L$) +H channels (see Tab. 2).

Since the collision potentials between hydrogen and the highly excited ionic Li-states considered here are not accessible by rigorous ab initio calculations, a model potential approach discussed in the following section is applied here.

2 Model approach

In the present work, model estimates for inelastic cross sections and rate coefficients are obtained within the standard Born–Oppenheimer formalism, which is the most widely used and reliable approach for theoretical studies of low-energy heavy-particle collisions. The approach treats a collision problem in two steps: a fixed-nuclei electronic structure calculation and a nonadiabatic nuclear dynamical treatment.

The adiabatic potentials are estimated in the present work by means of the model asymptotic approach described in reference [17]. It has been justified by the full quantum calculations for several collisional systems involving hydrogen [12,13,18–22] that the main mechanism of partial processes with high and moderate cross sections and rate coefficients is determined by the long-range ionic-covalent interactions. The model asymptotic approach [17] allows one to describe long-range nonadiabatic regions due to ionic-covalent interactions. In this case, nonadiabatic regions are passed by the system in a particular order and one can use the quantum multichannel model [14,23–26] in order to treat a nonadiabatic nuclear dynamics. This model is advantageous because it is analytical. Comparison with the previous quantum calculations has shown that the model approach to nonadiabatic nuclear dynamics provides reasonable estimates for inelastic cross sections and rate coefficients with large and moderate values [22,25].

The alternative approach for the nonadiabatic nuclear dynamics is the branching-probability-current method [17], which allows one to take into account not only long-range, but also short-range nonadiabatic regions, in particular, due to covalent–covalent interactions. It has been shown [17,27] that inclusion of short-range regions practically does not change rate coefficients with the highest values, may affect up to some extent rate coefficients with moderate values, and usually changes markedly rate coefficients with low values.
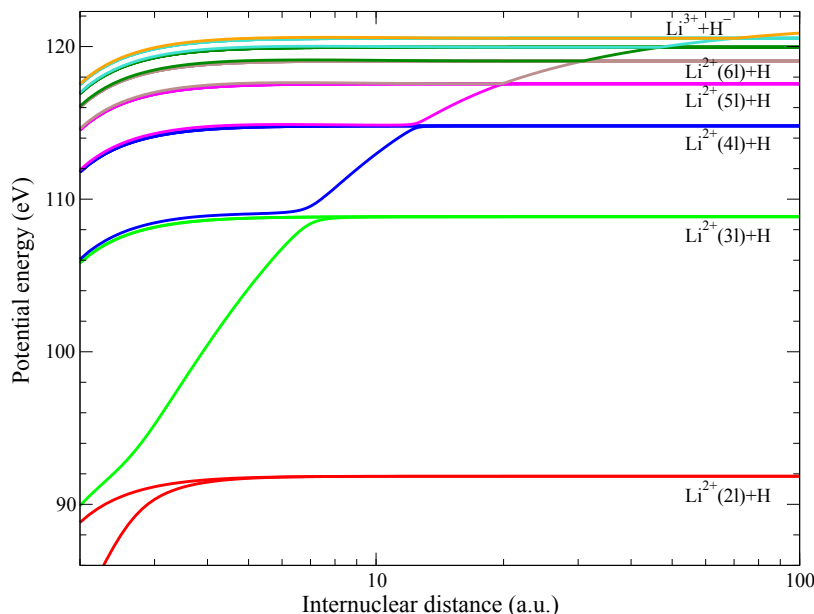
Fig. 1. The LiH^{2+}($^1\Sigma^+$) adiabatic potential energy curves obtained by means of the model approach. The potentials are measured from the ground state asymptote. The channels are defined in Table 1.

Since the main goal of the present paper is to calculate rate coefficients with the highest values, the multichannel model is employed in the present work based on the long-range (asymptotic) adiabatic potentials. Nonadiabatic transition probabilities in each nonadiabatic region are calculated within the Landau–Zener model by means of the adiabatic-potential-based formula [17,28]. Inelastic cross sections and rate coefficients for recombination, ion-pair formation, excitation and de-excitation processes are then calculated as usual.

3 Results for inelastic collisions Li^{3+} + H$^-$ and Li^{2+}(nl) + H

The scattering channels treated in the present study of inelastic collisions Li^{3+} + H$^-$ and Li^{2+}(nl) + H are listed in Table 1. Since the ground ionic molecular state, which is responsible for inelastic transitions, has $^1\Sigma^+$ symmetry, only the scattering channels with this molecular symmetry are taken into account. Molecular states of other symmetries are not included in the present consideration.

The table also provides the asymptotic energies of the scattering channels. They are given relative to the Li^{2+} + H asymptote for the molecular ion. The table shows that there is a large energy gap between this asymptote and the asymptote for the first excited state of the lithium ion Li^{2+}($2s$ ^2S) interacting with a hydrogen atom. In this gap an infinite number of Rydberg-like excited states Li^{2+}($1s$ ^2S) + H(nl) and Li$^+$($1snl$) + H$^+$ exist ($n \geq 2$). Above this group of Rydberg states the molecular states involving excited lithium ion states Li^{2+}(nl ^2L) interacting with hydrogen atoms are located together with the ion-pair state Li^{3+} + H$^-$, as listed in Table 1. The two groups are energetically well separated, there are thus no nonadiabatic transitions between states belonging to

the different groups. Transitions within each group can be studied independently. The present study treats nonadiabatic transitions between molecular states listed in Table 1 except the far low-lying Li^{2+} + H asymptote.

It is also worth to mention that the treated states are located in the Li^{2+}($1s$ ^2S) + H$^+$ + e^- continuum, so strictly speaking, these states are quasi-stationary. Nevertheless, using the approach from [30], it is possible to show that quasi-stationary widths of these states are negligible due to two-electron transitions and large internuclear distances. Thus, at the long-range distances, which are of the primary interest, the treated states can be considered as stationary, which is asymptotically exact.

The LiH^{2+}($^1\Sigma^+$) adiabatic potential energy curves calculated by the model approach described in the previous section are plotted in Figure 1. Short-range potentials estimated by this approach are not shown because only the long-range potentials determine essentially the low-energy collision rate coefficients with large and moderate values. A series of avoided crossings due to the ionic-covalent interactions is clearly seen. Since the nonadiabatic regions are located in a particular order, the multichannel nuclear dynamical approach is applicable here. As described above, a nonadiabatic transition probability in each nonadiabatic region is calculated by means of the adiabatic-potential-based formula within the Landau–Zener model. The multichannel analytic formulae [26] are then used for computing an inelastic probability for each state-to-state transition. Finally, the inelastic cross sections and rate coefficients are calculated for all transitions between the scattering channels collected in Table 1.

Charge recombination rate coefficients for the Li^{3+} + H$^-$ collisions are calculated by the model approach described above. It turns out that among all possible partial recombination processes according to Table 1 the high rate coefficients of the order of 10^{-8} cm^3/s are obtained
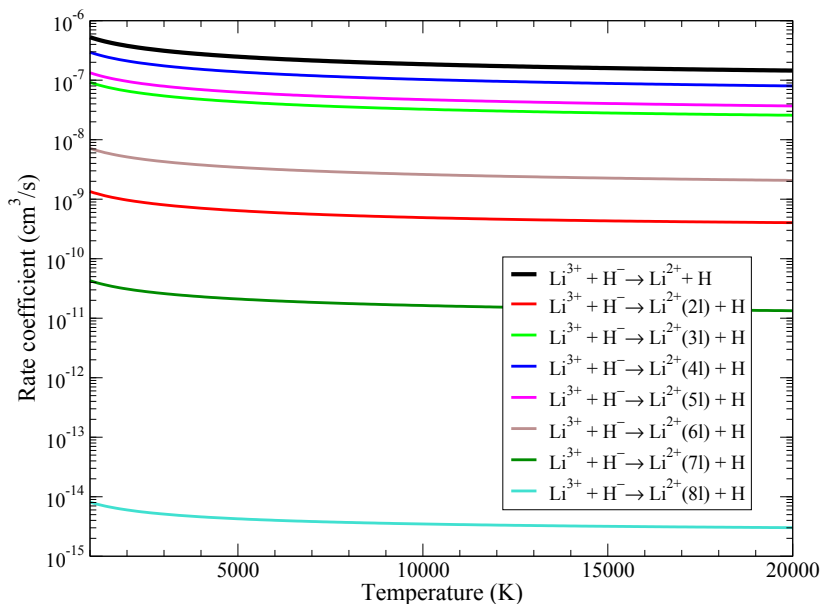
Fig. 2. Rate coefficients for the recombination processes in $Li^{3+} + H^-$ collisions. The initial channel is ionic, the final channels are defined in Table 1. The thick black curve represents the total (summed over all final channels) rate coefficient. The colored lines show rate coefficients for a given n of final channels $Li^{2+}(nl) + H$ summed over the quantum numbers l.
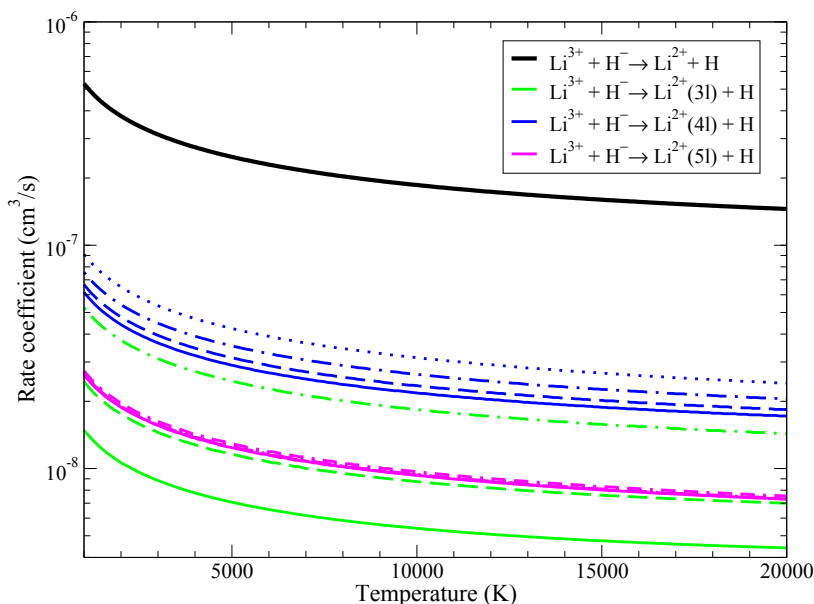

Fig. 3. The highest partial and total rate coefficients for recombination processes in $Li^{3+} + H^-$ collisions. The solid lines represent $Li^{2+}(ns)$ final states, the long-dashed lines $Li^{2+}(np)$, the dot-dashed $Li^{2+}(nd)$, the dotted lines $Li^{2+}(nf)$, the dot-double-dashed lines $Li^{2+}(ng)$, the double-dot-dashed lines $Li^{2+}(nh)$, the dashed lines $Li^{2+}(ni)$.

only for a smaller group of processes whereas rate coefficients for the remaining recombination processes are separated from these by at least an order of magnitude, see Figure 2. Notice that this figure shows rate coefficients summed over quantum numbers l at a given n for the final channels. The temperature dependences of the recombination rate coefficients with the highest values corresponding to the partial processes into the $Li^{2+}(3l, 4l, 5l)$ final states are plotted in Figure 3 for a wide temperature range up to $T = 20\,000\,K$. Table 3 presents actual

numerical rate coefficient values for these most intensively populated states in $Li^{3+} + H^-$ and $Li^{2+}(nl) + H$ collisions at a temperature of $T = 10\,000\,K$. All the partial rate coefficients contribute to the total recombination rate coefficient exceeding $2 \times 10^{-7}\,cm^3/s$. The highest rate coefficients for the partial recombination processes correspond to those processes leading to the $Li^{2+}(4l)$ final states. At $T = 10\,000\,K$ the rate coefficients for these states vary between $2.18 \times 10^{-8}\,cm^3/s$ and $3.14 \times 10^{-8}\,cm^3/s$. For recombination processes into

Table 2. LiH$^+$($^2\Sigma^+$) scattering channels and asymptotic energies (J-average experimental values taken from NIST [29]) with respect to the ground state.

j	Scattering (atomic) channels	Asymptotic energies (eV)
1	Li$^+$ ($1s^2$ ^1S) + H ($1s$ ^2S)	0.0000000
2	Li$^+$ ($1s2s$ ^3S) + H ($1s$ ^2S)	59.020815
3	Li$^+$ ($1s2s$ ^1S) + H ($1s$ ^2S)	60.922690
4	Li$^+$ ($1s2p$ ^3P) + H ($1s$ ^2S)	61.280805
5	Li$^+$ ($1s2p$ ^1P) + H ($1s$ ^2S)	62.216335
6	Li$^+$ ($1s3s$ ^3S) + H ($1s$ ^2S)	68.780785
7	Li$^+$ ($1s3s$ ^1S) + H ($1s$ ^2S)	69.279627
8	Li$^+$ ($1s3p$ ^3P) + H ($1s$ ^2S)	69.369302
9	Li$^+$ ($1s3d$ ^3D) + H ($1s$ ^2S)	69.585346
10	Li$^+$ ($1s3d$ ^1D) + H ($1s$ ^2S)	69.589059
11	Li$^+$ ($1s3p$ ^1P) + H ($1s$ ^2S)	69.648473
12	Li$^+$ ($1s4s$ ^3S) + H ($1s$ ^2S)	71.908520
13	Li$^+$ ($1s4s$ ^1S) + H ($1s$ ^2S)	72.108809
14	Li$^+$ ($1s4p$ ^3P) + H ($1s$ ^2S)	72.144710
15	Li$^+$ ($1s4d$ ^3D) + H ($1s$ ^2S)	72.234885
16	Li$^+$ ($1s4d$ ^1D) + H ($1s$ ^2S)	72.237031
17	Li$^+$ ($1s4f$ ^3F) + H ($1s$ ^2S)	72.238521
18	Li$^+$ ($1s4f$ ^1F) + H ($1s$ ^2S)	72.238654
19	Li$^+$ ($1s4p$ ^1P) + H ($1s$ ^2S)	72.261723
20	Li$^+$ ($1s5s$ ^3S) + H ($1s$ ^2S)	73.297506
21	Li$^+$ ($1s5s$ ^1S) + H ($1s$ ^2S)	73.397349
22	Li$^+$ ($1s5p$ ^3P) + H ($1s$ ^2S)	73.415303
23	Li$^+$ ($1s5d$ ^3D) + H ($1s$ ^2S)	73.461173
24	Li$^+$ ($1s5d$ ^1D) + H ($1s$ ^2S)	73.462426
25	Li$^+$ ($1s5f$ ^3F) + H ($1s$ ^2S)	73.463130
26	Li$^+$ ($1s5f$ ^1F) + H ($1s$ ^2S)	73.463254
27	Li$^+$ ($1s5p$ ^1P) + H ($1s$ ^2S)	73.477364
28	Li$^+$ ($1s6s$ ^3S) + H ($1s$ ^2S)	74.033686
29	Li$^+$ ($1s6s$ ^1S) + H ($1s$ ^2S)	74.090542
30	Li$^+$ ($1s6p$ ^3P) + H ($1s$ ^2S)	74.100775
31	Li$^+$ ($1s6p$ ^1P) + H ($1s$ ^2S)	74.122200
32	Li$^+$ ($1s6d$ ^3D) + H ($1s$ ^2S)	74.127197
33	Li$^+$ ($1s6d$ ^1D) + H ($1s$ ^2S)	74.127984
34	Li$^+$ ($1s6f$ ^3F) + H ($1s$ ^2S)	74.128345
35	Li$^+$ ($1s6f$ ^1F) + H ($1s$ ^2S)	74.128475
i	Li^{++} ($1s$ ^2S) + H$^-$ ($1s^2$ ^1S)	74.885893

Obviously recombinations are much more efficient than any other processes in this collisional system.

Rate coefficients K_{fi} for an endothermic ion-pair formation process $f \rightarrow i$ are evaluated here by the detailed balance relation using the rate coefficient K_{if} for the corresponding exothermic process $i \rightarrow f$ applying the following equation

$$K_{fi}(T) = K_{if}(T) \frac{p_f^{stat}}{p_i^{stat}} \exp\left(-\frac{\Delta E_{if}}{k_B T}\right), \qquad (1)$$

$\Delta E_{if} = E_i - E_f$ being the energy defect which is positive for an endothermic process $f \rightarrow i$, p_j^{stat} a statistical probability of a channel j, and k_B the Boltzmann constant. Equation (1) determines the temperature dependence of the ion-pair formation processes taking into account that the recombination rate coefficients are slowly varying with temperature.

The temperature dependence of the rate coefficients for the ion-pair formation processes as inverse of the corresponding most efficient recombination processes are plotted in Figure 4 for the temperature range up to $T = 20\,000$ K. Due to the endothermicity of the ion-pair formation processes their rate coefficient curves have large energy thresholds and their maximum values are orders of magnitude smaller compared to their recombination equivalences. Actual numerical values at the temperature of $T = 10\,000$ K can be obtained from Table 3.

The calculated partial rate coefficients for all processes in ionic-lithium–hydrogen collisions between the states listed in Table 1 are available online as supplementary materials to this paper.

It can be speculated here that at high enough H$^-$ abundances the charge recombination processes Li^{3+} + H$^-$ $\rightarrow$ Li$^{2+}(nl)$ + H can quickly lead to the formation of the excited ions Li$^{2+}(3l, 4l, 5l)$ due to the rather large charge recombination rate coefficients. The excited lithium ions will then produce ground-state lithium ions Li^{2+} in cascade transitions. If H$^-$ abundances are low, the electron recombination processes can produce excited ions Li$^{2+}(nl)$, and the ion-pair formation processes in collisions of these ions with neutral hydrogen atoms efficiently create H$^-$ anions, which are important for many processes in astrophysics. In any case, charge recombination processes in Li^{3+} + H$^-$ collisions and their inverse processes, the ion-pair formation, can possibly compete with electron recombination processes in the formation of lithium ions and atoms, as well as in the production of hydrogen negative ions.

the Li$^{2+}(3l)$ states the rate coefficients are slightly lower, varying between 5.40×10^{-9} cm^3/s and 1.84×10^{-8} cm^3/s whereas for the processes ending in the Li$^{2+}(5l)$ final states they are in the range of 9×10^{-9} cm^3/s.

Table 3 presents the rate coefficients at $T = 10\,000$ K for all transitions between the most intensively populated states in Li^{3+} + H$^-$ and Li$^{2+}(nl)$ + H collisions. From the table it follows that the largest recombination rate coefficients are at least 20 times higher than the rate coefficients for excitation and de-excitation processes. At $T = 10\,000$ K the maximum rate coefficients for the de-excitation process Li$^{2+}(4s \rightarrow 3d)$ + H are equal to 8.68×10^{-10} cm^3/s whereas 6.67×10^{-10} cm^3/s for the excitation process Li$^{2+}(4s \rightarrow 4p)$ + H. Rate coefficients for the ion-pair formation processes are at least 500 times smaller compared to the recombination processes. According to Table 3 the maximum ion-pair formation rate coefficient at $T = 10\,000$ K is equal to 1.90×10^{-11} cm^3/s.

4 Results for inelastic collisions Li^{2+} + H$^-$ and Li$^+(1snl)$ + H

The ground ionic molecular state Li^{2+} + H$^-$ has $^2\Sigma^+$ symmetry. Therefore, it is sufficient to treat nonadiabatic transitions only within this molecular symmetry when estimating inelastic cross sections and rate coefficients with high and moderate values. Similar to the previously discussed situation in LiH^{2+}, there are two energetically

Table 3. Rate coefficients, in units of cm^3/s, for the most important inelastic processes at $T = 10\,000$ K, that is, for the recombination processes in Li^{3+} + H$^-$ collisions, as well as for the ion-pair formation, excitation, and de-excitation processes in Li$^{2+}(nl)$ + H collisions. The labels for the initial and the final states are listed in Table 1.

Initial states	Final states						
	4	5	6	7	8	9	10
$T = 10\,000$ K							
4	–	2.44E−10	4.38E−11	1.75E−13	8.55E−14	6.28E−14	5.42E−14
5	8.13E−11	–	7.46E−11	1.16E−13	5.50E−14	3.99E−14	3.42E−14
6	8.77E−12	4.48E−11	–	1.74E−13	7.96E−14	5.71E−14	4.86E−14
7	1.75E−10	3.47E−10	8.68E−10	–	6.67E−10	4.22E−10	3.38E−10
8	2.85E−11	5.50E−11	1.33E−10	2.22E−10	–	2.28E−10	1.67E−10
9	1.26E−11	2.39E−11	5.70E−11	8.44E−11	1.37E−10	–	1.76E−10
10	7.75E−12	1.47E−11	3.47E−11	4.83E−11	7.17E−11	1.26E−10	–
11	3.47E−11	6.13E−11	1.38E−10	1.32E−10	1.49E−10	1.77E−10	2.19E−10
12	9.38E−12	1.65E−11	3.68E−11	3.45E−11	3.89E−11	4.58E−11	5.64E−11
13	5.51E−12	9.69E−12	2.16E−11	2.03E−11	2.29E−11	2.69E−11	3.31E−11
14	3.89E−12	6.83E−12	1.52E−11	1.43E−11	1.61E−11	1.89E−11	2.33E−11
15	3.03E−12	5.32E−12	1.19E−11	1.11E−11	1.25E−11	1.47E−11	1.81E−11
i	5.40E−09	8.74E−09	1.84E−08	2.18E−08	2.35E−08	2.64E−08	3.14E−08

| Initial states	Final states					
	11	12	13	14	15	i
$T = 10\,000$ K						
4	1.42E−15	1.15E−15	1.13E−15	1.11E−15	1.11E−15	4.50E−16
5	8.36E−16	6.74E−16	6.60E−16	6.51E−16	6.52E−16	2.43E−16
6	1.13E−15	9.04E−16	8.85E−16	8.73E−16	8.74E−16	3.07E−16
7	5.39E−12	4.23E−12	4.14E−12	4.08E−12	4.09E−12	1.82E−12
8	2.04E−12	1.59E−12	1.56E−12	1.53E−12	1.54E−12	6.52E−13
9	1.45E−12	1.12E−12	1.10E−12	1.08E−12	1.08E−12	4.40E−13
10	1.28E−12	9.88E−13	9.66E−13	9.51E−13	9.52E−13	3.74E−13
11	–	8.37E−11	7.78E−11	7.44E−11	7.46E−11	1.90E−11
12	2.79E−11	–	2.89E−11	2.71E−11	2.73E−11	6.36E−12
13	1.56E−11	1.74E−11	–	1.84E−11	1.87E−11	3.84E−12
14	1.06E−11	1.16E−11	1.31E−11	–	1.70E−11	2.77E−12
15	8.29E−12	9.10E−12	1.04E−11	1.32E−11	–	2.19E−12
i	9.32E−09	9.35E−09	9.42E−09	9.52E−09	9.68E−09	–
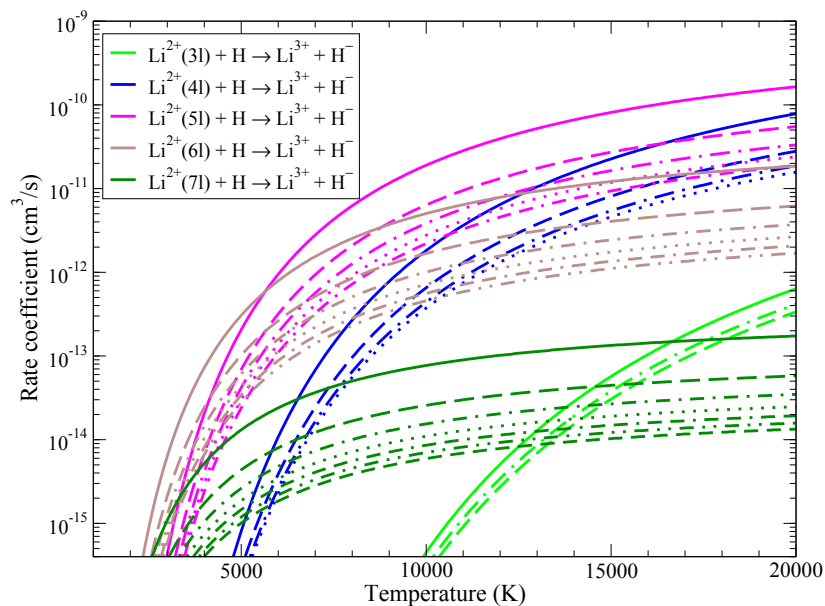
Fig. 4. The partial rate coefficients for ion-pair formation processes in Li$^{2+}(nl)$ + H collisions. The labels for the initial channels are the same as in Figure 3 for the final channels of the recombination processes.

Table 4. Rate coefficients, in units of cm^3/s, for the most important inelastic processes at $T = 10\,000$ K, that is, for the recombination processes in $Li^{2+} + H^-$ collisions, as well as for the ion-pair formation, excitation, and de-excitation processes in $Li^+(1snl) + H$ collisions. The labels for the initial and the final channels are listed in Table 2.

Initial states	Final states							
	6	7	8	9	10	11	12	13
				$T = 10\,000$ K				
6	–	1.01E−09	1.91E−10	5.44E−11	1.76E−11	7.13E−12	6.10E−13	3.83E−13
7	5.41E−09	–	2.77E−09	6.54E−10	1.87E−10	7.09E−11	5.41E−12	3.30E−12
8	1.26E−10	3.42E−10	–	3.07E−10	6.80E−11	2.27E−11	1.43E−12	8.35E−13
9	2.77E−11	6.22E−11	2.37E−10	–	1.97E−10	5.40E−11	2.61E−12	1.47E−12
10	2.70E−11	5.37E−11	1.58E−10	5.94E−10	–	6.35E−10	2.00E−11	1.07E−11
11	1.95E−11	3.63E−11	9.42E−11	2.90E−10	1.13E−09	–	9.79E−11	5.00E−11
12	2.30E−11	3.81E−11	8.15E−11	1.93E−10	4.91E−10	1.35E−09	–	8.52E−10
13	5.47E−11	8.80E−11	1.81E−10	4.11E−10	9.98E−10	2.61E−09	3.22E−09	–
14	5.39E−12	8.58E−12	1.73E−11	3.88E−11	9.26E−11	2.37E−10	2.64E−10	3.74E−10
15	2.25E−12	3.55E−12	7.09E−12	1.57E−11	3.69E−11	9.31E−11	9.09E−11	1.04E−10
16	6.27E−12	9.83E−12	1.95E−11	4.28E−11	9.99E−11	2.50E−10	2.37E−10	2.60E−10
17	1.40E−12	2.19E−12	4.32E−12	9.43E−12	2.19E−11	5.44E−11	5.00E−11	5.30E−11
18	4.09E−12	6.39E−12	1.26E−11	2.74E−11	6.33E−11	1.57E−10	1.42E−10	1.49E−10
19	9.76E−12	1.52E−11	2.99E−11	6.51E−11	1.51E−10	3.74E−10	3.36E−10	3.51E−10
i	1.19E−09	1.66E−09	2.80E−09	5.25E−09	1.05E−08	2.30E−08	2.07E−08	1.89E−08

Initial states	Final states						
	14	15	16	17	18	19	i
				$T = 10\,000$ K			
6	3.26E−13	2.04E−13	1.89E−13	1.78E−13	1.73E−13	1.72E−13	3.33E−13
7	2.78E−12	1.73E−12	1.59E−12	1.49E−12	1.44E−12	1.43E−12	2.48E−12
8	6.92E−13	4.25E−13	3.88E−13	3.61E−13	3.50E−13	3.48E−13	5.16E−13
9	1.19E−12	7.24E−13	6.57E−13	6.07E−13	5.87E−13	5.83E−13	7.46E−13
10	8.59E−12	5.13E−12	4.62E−12	4.25E−12	4.10E−12	4.07E−12	4.52E−12
11	3.93E−11	2.31E−11	2.07E−11	1.89E−11	1.81E−11	1.80E−11	1.76E−11
12	6.02E−10	3.11E−10	2.70E−10	2.38E−10	2.26E−10	2.23E−10	2.18E−10
13	3.23E−09	1.34E−09	1.12E−09	9.57E−10	8.97E−10	8.81E−10	7.52E−10
14	–	2.05E−10	1.62E−10	1.34E−10	1.24E−10	1.21E−10	9.32E−11
15	1.36E−10	–	1.36E−10	8.85E−11	7.83E−11	7.40E−11	4.61E−11
16	3.25E−10	4.10E−10	–	3.55E−10	2.95E−10	2.69E−10	1.46E−10
17	6.39E−11	6.35E−11	8.46E−11	–	9.71E−11	8.00E−11	3.66E−11
18	1.78E−10	1.68E−10	2.11E−10	2.91E−10	–	3.31E−10	1.18E−10
19	4.16E−10	3.82E−10	4.61E−10	5.75E−10	7.92E−10	–	3.09E−10
i	2.02E−08	1.50E−08	1.57E−08	1.66E−08	1.78E−08	1.95E−08	–

well separated groups of molecular states in LiH^+. Apart from the first group which includes the LiH^+ ground state as well as an infinite number of Rydberg-like excited states $Li^+(1s^2) + H(nl)$ and $Li(1s^2nl) + H^+$, the second group of scattering channels, as listed in Table 2, consists of $Li^+(1snl) + H$ states ($n \geq 2$) plus the ion-pair state $Li^{2+} + H^-$. Because of the large energy gap between the two groups, nonadiabatic transitions between molecular states from the different groups can be neglected. Nonadiabatic transitions between low-lying states in the first group have been studied previously by [15,16], as mentioned above. The present study of inelastic $Li^{2+} + H^-$ and $Li^+ + H$ collisions is performed for 35 scattering channels leading to the 34 excited $Li^+(1snl\ ^{1,3}L)$ states ($n \geq 2$) below the Li^{2+} ionization limit interacting with the hydrogen atom, as well as the ionic pair $Li^{2+} + H^-$ in its ground state (Tab. 2). Like in the case of LiH^{2+}, quasi-stationary widths of the treated molecular states are negligible.

The asymptotic model adiabatic potentials for the LiH^+ ($^2\Sigma^+$) molecule are plotted in Figure 5. A series of avoided crossings due to the ionic-covalent interactions is clearly seen. Landau–Zener parameters in each nonadiabatic region are determined using the adiabatic-potential-based formula [17,28] followed by calculations of nonadiabatic transition probabilities with the multichannel formula [24,26]. Inelastic cross sections and rate coefficients for the recombination processes due to the transitions between the states listed in Table 2 are then calculated as usual.

The temperature dependences of rate coefficients with large and moderate values for the charge recombination processes in $Li^{2+} + H^-$ collisions are plotted in Figure 6. In the upper part of the figure there is a series of partial processes with high rate coefficients which correspond to the recombination processes into the final states Li^+ ($1s3d\ ^1D$), Li^+ ($1s3p\ ^1P$), Li^+ ($1s4s\ ^{1,3}S$),

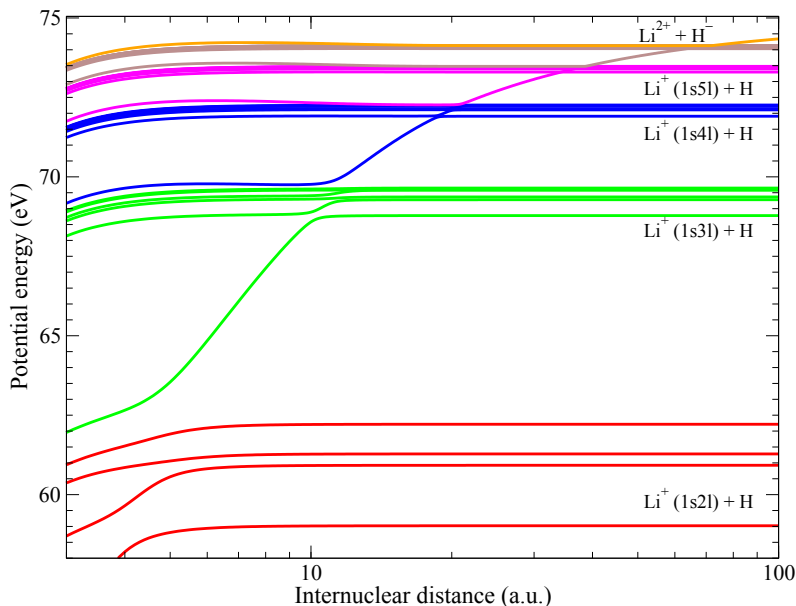**Fig. 5.** The LiH$^+$($^2\Sigma^+$) adiabatic potential energy curves obtained by means of the model approach. The potentials are measured from the ground state asymptote. The potential channels are defined in Table 2.

Li$^+$ (1s4p $^{1,3}P$), Li$^+$ (1s4d $^{1,3}D$), Li$^+$ (1s4f $^{1,3}F$). The rate coefficient values of these recombination processes are of the order of magnitude of 10^{-8} cm^3/s. Actual numerical values for these rate coefficients at temperature $T = 10\,000$ K are summarized in Table 4. Below this group a number of recombination processes with moderate rate coefficients appear, with values between 10^{-10} and 10^{-8} cm^3/s. Other rate coefficients with values smaller than 10^{-10} cm^3/s are not shown in the figure. The calculated partial rate coefficients for all processes in ionic-lithium–hydrogen collisions between the states listed in Table 2 are available online as supplementary materials to this paper. For the total recombination rate coefficient (the thick black curve) at temperature $T = 10\,000$ K a value equal to 2×10^{-7} cm^3/s is obtained, which practically coincides with the total recombination rate coefficient in Li^{3+} + H$^-$ collisions.

Like in the LiH^{2+} collisional system, rate coefficients for the ion-pair formation, excitation and de-excitation processes are smaller than their recombination analogs. Differences however are not as large here. According to Table 4 and Figure 7, the highest rate coefficients for ion-pair formation, excitation and de-excitation processes in the LiH$^+$ system are only about one order of magnitude smaller compared to the largest recombination rate coefficients. This is due to smaller energy defects in the LiH$^+$ collisional system compared to the LiH^{2+} system. Determinations of the ion-pair formation rate coefficients K_{fi} are done again applying relation (1), using the corresponding recombination rate coefficients K_{if}. Since the energy thresholds ΔE_{if} are here not as large as for similar processes in Li$^{2+}(nl)$ + H collisions, ion-pair formation rate coefficients in Li$^+(1snl)$ + H collisions are obtained with larger values (Fig. 7). For higher temperatures several partial ion-pair formation rate coefficients in Li$^+(1snl)$ + H

collisions can become larger than 10^{-9} cm^{3}s^{-1} which is roughly an order of magnitude higher than in Li$^{2+}(nl)$ + H collisions (Fig. 4).

The high rate coefficient values obtained here show that charge recombination and the inverse processes, ion-pair formation, in Li^{2+} + H$^-$ and Li$^+(1snl)$ + H collisions are efficient in producing Li$^+$ ions, as well as H$^-$ anions. Therefore, like in Li^{3+} + H$^-$ and Li$^{2+}(nl)$ + H collisions, it can be guessed that at high H$^-$ abundances the charge recombination Li^{2+} + H$^-$ → Li$^+(1snl)$ + H can effectively produce excited lithium ions Li$^+$(1s3l, 1s4l) which quickly cascade down to ground-state ions Li$^+$(1s^2), where mutual neutralization in collisions with hydrogen negative ions finally results in production of lithium atoms. If the abundance of H$^-$ is low, electron recombination processes can create excited ions Li$^+(1snl)$ which through collisions with neutral hydrogen atoms can efficiently increase the abundance of H$^-$ anions due to high rate coefficients of the ion-pair formation processes. The same expectations can therefore be formulated as in the case of Li^{3+} + H$^-$ and Li$^{2+}(nl)$ + H collisions, that formation of lithium ions and atoms as well as production of hydrogen negative ions could be influenced by the present collisional processes.

5 Conclusion

Inelastic processes in low-energy collisions in the systems Li^{3+} + H$^-$, Li^{2+} + H and Li^{2+} + H$^-$ and Li$^+$ + H are investigated for all collisional channels with the excited ionic lithium states Li$^{2+}(nl)$ and Li$^+(1s\,nl)$ up to and including the corresponding ion-pair states. Since the collision potentials between hydrogen and the highly excited lithium ions considered here are not accessible by rigorous ab initio calculations, a model potential approach
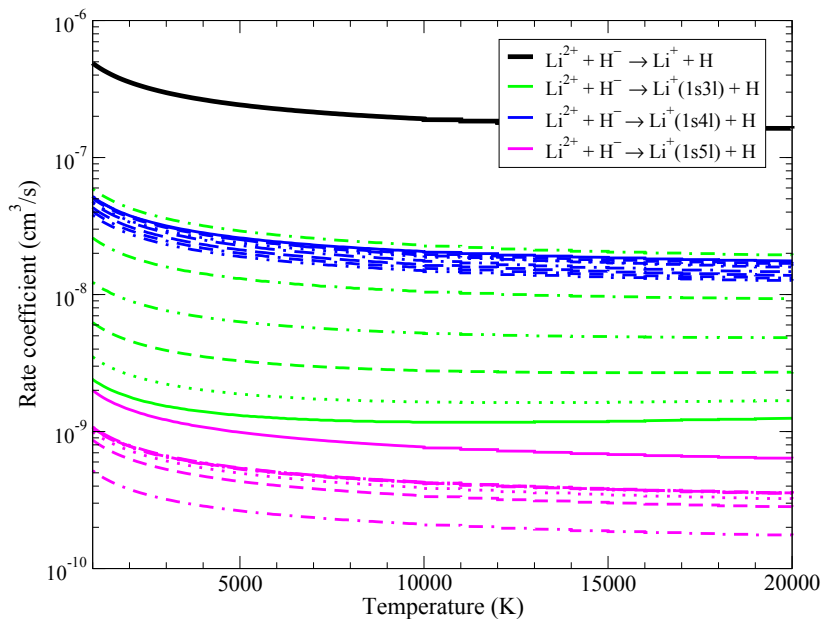
Fig. 6. Partial rate coefficients for recombination processes in $Li^{2+} + H^-$ collisions with high and moderate values. The thick black line shows the total recombination rate coefficient. The initial channel is ionic. For the final channels, solid curves represent $Li^+(1sns\ ^3S) + H$ states, dotted curves $Li^+(1sns\ ^1S) + H$, dashed curves $Li^+(1snp\ ^3P) + H$, dot-dashed curves $Li^+(1snp\ ^1P) + H$, double-dot-dashed curves $Li^+(1snd\ ^3D) + H$, dot-double-dashed curves $Li^+(1snd\ ^1D) + H$, long-dashed curves $Li^+(1snf\ ^3F) + H$, dot-long-dashed curves $Li^+(1snf\ ^1F) + H$.
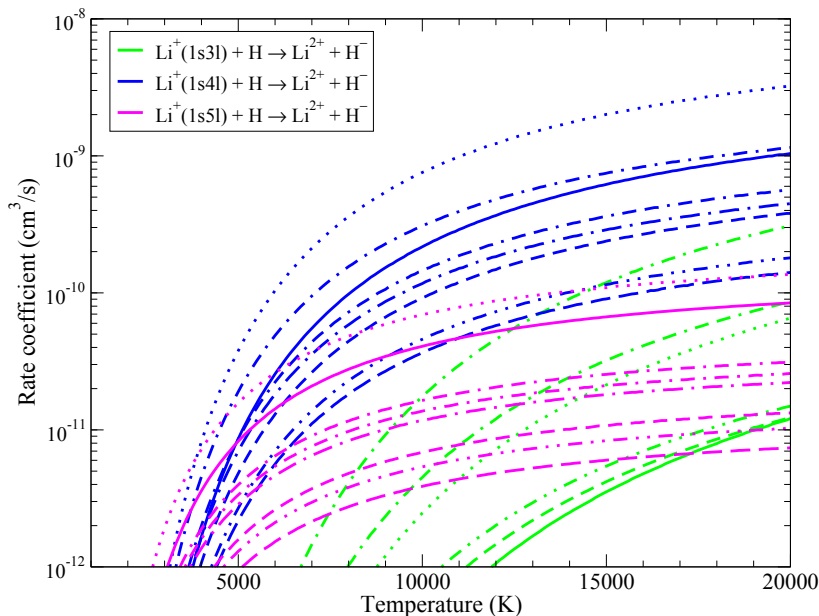
Fig. 7. The partial rate coefficients for ion-pair formation processes in $Li^+(1snl) + H$ collisions. The labels for the initial channels are the same as in Figure 6 for the final channels of the recombination processes.

is applied. Based on the long-range asymptotic adiabatic potentials the multichannel model is employed. Nonadiabatic transition probabilities in each nonadiabatic region are calculated within the Landau–Zener model using the adiabatic-potential-based formula. Inelastic cross sections are obtained and used to calculate rate coefficients for recombination, ion-pair formation, excitation and deexcitation processes.

For both collisional systems total rate coefficients for the charge recombination processes are determined with maximum values between 10^{-7} cm^3/s and 10^{-6} cm^3/s over a wide temperature range at least up to $T = 20\,000$ K.

In case of the inverse, ion-pair formation, processes rate coefficients in both collisional systems start for temperatures much below $T = 1000\,\mathrm{K}$ at small values due to their endothermicity, but with increasing temperatures the rate coefficients for several partial processes are rapidly increasing reaching maximum values of the order of $10^{-10} - 10^{-9}\,\mathrm{cm}^3/\mathrm{s}$ at temperatures close to $T = 20\,000\,\mathrm{K}$.

With their large rate coefficient values the charge recombinations and their inverse processes, the ion-pair formations, are thus found to be very efficient in producing lithium cations and/or hydrogen anions in both collisional systems discussed here. But in spite of this finding, the probability that the formation of Li^{Z+} and H^- ions in interstellar or stellar-atmosphere environments could be influenced by these collisional processes is very low due to the fact that under conditions where the multiply charged lithium ions exist the H^- ions are readily destroyed. We assume that the present results are important from a fundamental point of view, most likely the results on the charge recombination constitute useful predictions for possible upcoming experiments, as well as possible applications, and therefore, the rate coefficients are calculated and presented for all processes in the considered collisions for completeness of the data.

Author contribution statement

All the authors were involved in the preparation of the manuscript. All the authors have read and approved the final manuscript. All the authors equally contributed into the present work.

References

1. R. Morgenstern, T. Schlatholter, R. Hoekstra, in *The Physics of Electronic and Atomic Collisions (21st International Conference on the Physics of Electronic and Atomic Collisions (21st ICPEAC), Sendai, Japan, 1999)* (2000), Vol. 500, pp. 65–84
2. G. Lubinski, Z. Juhasz, R. Morgenstern, R. Hoekstra, Phys. Rev. Lett. **86**, 616 (2001)
3. U. Kadhane, D. Misra, Y.P. Singh, L.C. Tribedi, Phys. Rev. Lett. **90**, 093401 (2003)
4. R.D. Thomas, H.T. Schmidt, G. Andler et al., Rev. Sci. Instrum. **82**, 065112 (2011)
5. H.T. Schmidt, R.D. Thomas, M. Gatchell et al., Rev. Sci. Instrum. **84**, 055115 (2013)
6. R. von Hahn, A. Becker, F. Berg, K. Blaum, C. Breitenfeldt, H. Fadil, F. Fellenberger, M. Froese, S. George, J. Göck et al., Rev. Sci. Instrum. **87**, 063115 (2016)
7. Y. Nakano, Y. Enomoto, T. Masunaga, S. Menk, P. Bertier, T. Azuma, Rev. Sci. Instrum. **88**, 033110 (2017)
8. M. Asplund, Annu. Rev. Astron. Astrophys. **43**, 481 (2005)
9. L. Mashonkina, IAU Symp. **298**, 355 (2014)
10. P.S. Barklem, Astron. Astrophys. Rev. **24**, 1 (2016)
11. P.S. Barklem, A.K. Belyaev, M. Asplund, Astron. Astrophys. **409**, L1 (2003)
12. H. Croft, A.S. Dickinson, F.X. Gadéa, J. Phys. B: At. Mol. Opt. Phys. **32**, 81 (1999)
13. H. Croft, A.S. Dickinson, F.X. Gadéa, MNRAS **304**, 327 (1999)
14. A.K. Belyaev, P.S. Barklem, Phys. Rev. A **68**, 062703 (2003)
15. L. Liu, C.H. Liu, G. Wang, R.K. Janev, Phys. Rev. A **84**, 032710 (2011)
16. L. Yan, Y. Qu, C. Liu, J. Wang, R.J. Buenker, J. Chem. Phys. **136**, 124304 (2012)
17. A.K. Belyaev, Phys. Rev. A **88**, 052704 (2013)
18. A.K. Belyaev, J. Grosser, J. Hahne, T. Menzel, Phys. Rev. A **60**, 2151 (1999)
19. A.K. Belyaev, P.S. Barklem, A.S. Dickinson, F.X. Gadéa, Phys. Rev. A **81**, 032706 (2010)
20. J.Z. Mezei, J.B. Roos, K. Shilyaeva, N. Elander, Å. Larson, Phys. Rev. A **84**, 012703 (2011)
21. A.K. Belyaev, P.S. Barklem, A. Spielfiedel, M. Guitou, N. Feautrier, D.S. Rodionov, D.V. Vlasov, Phys. Rev. A **85**, 032704 (2012)
22. M. Guitou, A. Spielfiedel, D.S. Rodionov, S.A. Yakovleva, A.K. Belyaev, T. Merle, F. Thévenin, N. Feautrier, Chem. Phys. **462**, 94 (2015)
23. A.K. Belyaev, S.I. Tserkovnyi, Opt. Spektrosk. **63**, 968 (1987)
24. A.K. Belyaev, Phys. Rev. A **48**, 4299 (1993)
25. A.K. Belyaev, S.A. Yakovleva, P.S. Barklem, Astron. Astrophys. **572**, A103 (2014)
26. S.A. Yakovleva, Y.V. Voronov, A.K. Belyaev, Astron. Astrophys. **593**, A27 (2016)
27. A. Mitrushchenkov, M. Guitou, A.K. Belyaev, S.A. Yakovleva, A. Spielfiedel, N. Feautrier, J. Chem. Phys. **246**, 014304 (2017)
28. A.K. Belyaev, O.V. Lebedev, Phys. Rev. A **84**, 014701 (2011)
29. A. Kramida, Y. Ralchenko, J. Reader, NIST ASD Team, in *NIST Atomic Spectroscopy Database, Version 5.0* (National Institute of Standards and Technology, Gaithersburg, 2012), http://physics.nist.gov/asd
30. M. Satta, T. Grassi, F.A. Gianturco, S.A. Yakovleva, A.K. Belyaev, Mon. Not. R. Astron. Soc. **436**, 2722 (2013)